On the Transient Thermal Characteristics of Silicon Carbide Power Electronics Modules

Gary Mandrusiak, Xu She, *Senior Member, IEEE*, Alistair Martin Waddell, and Sayan Acharya, *Student Member, IEEE*

***Abstract*—The transient performance of power semiconductor devices relates directly to their available power rating, reliability, and operating lifetime. This paper examines the transient thermal performance of liquid-cooled, silicon carbide power devices subjected to different unsteady electrical loads. The first part uses infrared thermography to examine an observed asymmetrical device thermal time constant when subjected to step-change increases and decreases in current. A theoretical analysis connects this behavior to the dependence of MOSFET on-resistance on junction temperature. It also identifies three time constants that characterize junction transient response, one each for the die, the module, and the cold plate. The second part extends the transient thermal evaluation to half-sine wave periodic excitations that emulate real-application operating conditions. These experiments show that thermal ripple increases with increasing excitation amplitude but decreases with increasing excitation frequency. They also connect the observed thermal response to the time constants inferred from the step-change experiments. Both parts of the study show the importance of considering transient loads when designing power electronics cooling systems and the role that electrical properties play in determining unsteady thermal response.**

***Index Terms*—Silicon carbide (SiC) MOSFET, thermal management, transient thermal performance.**

NOMENCLATURE

A	Convection surface area (m^2).
c	Specific heat (J/kg. °C).
C_{Th}	Thermal capacitance (J/°C).
C_1, C_2, C_3	Coefficients in temperature curve fit.
f	Excitation frequency (Hz).
h	Convective heat transfer coefficient (W/m^2. °C).
I	Current (Amps).
ρ	Density (kg/m^3).
R_{Th}	Thermal resistance (°C/W).
R	Electrical resistance (Ohm).
R_0, R_1, R_2	Electrical Resistance Curve Fit.
T	Temperature at time t (°C).
T_{Initial}	Temperature at time $t = 0$ (°C).
T_{Final}	Temperature at steady state (°C).
T_A	Temperature of cooling fluid (°C).
t	Time (s).
τ	Time constant (s).
V	Volume (m^3).

Manuscript received September 21, 2017; revised December 19, 2017; accepted January 8, 2018. Date of publication March 1, 2018; date of current version August 7, 2018. Recommended for publication by Associate Editor A. Lindemann. *(Corresponding author: Xu She.)*

G. Mandrusiak and X. She are with the GE Global Research Center, Niskayuna, NY 12309 USA (e-mail: mandrusi@ge.com; xu.she@ge.com).

A. M. Waddell is with the GE Global Research Center, Munich 85754, Germany (e-mail: alistair.waddell@ge.com).

S. Archarya was with the GE Global Research Center, Niskayuna, NY 12309 USA. He is now with the North Carolina State University, Raleigh, NC 27606 USA (e-mail: sachary@ncsu.edu).

Color versions of one or more of the figures in this paper are available online at http://ieeexplore.ieee.org.

Digital Object Identifier 10.1109/TPEL.2018.2794919

I. INTRODUCTION

THE transient thermal performance of power semiconductor devices relates directly to their available power rating, reliability, and operating life. In power electronics systems, thermal effects contribute to over half of the sources of stress distribution that lead to failure [1]. Among these sources, thermal cycling is one of the most typical, with both fluctuations in thermal loads and mismatches in coefficients of thermal expansion contributing to failure [2]. As a result, understanding transient thermal characteristics is critical in guiding the design of high-performance power electronics systems. In recent years, silicon carbide (SiC) has emerged as a popular replacement for silicon in next-generation power devices. SiC offers higher electron mobility, faster switching speed, wider bandgap, higher dielectric breakdown, and higher allowable operating temperatures [3]–[5]. However, the smaller size of the SiC chip and the correspondingly larger current density makes cooling of SiC power devices a challenge. Over the years, the electronics cooling community has developed different technologies to manage device waste heat [6], including concepts that use air [7], liquid [8], [9], and phase-change [10]. These technologies are generally verified for steady-state dc conditions, which represent the nominal power dissipation in an application. This characterization is more than adequate for most installations, especially those for which the duration of any transient excitation is relatively short. In some applications, however, system performance is limited by the transient thermal characteristics of the module. This is especially true when modules are used in low-frequency operations, such as during the fault ride through of the doubly fed induction generator wind system, for which the electrical load changes at rates comparable to the module thermal time constant [11], [12]. In cases like this, peak temperatures caused by thermal fluctuations may require the module be derated during operation to ensure adequate reliability.

Power device lifetime can also be affected by the number of cycles operating at very low frequency with large ripple [13].

See http://www.ieee.org/publications_standards/publications/rights/index.html for more information.

Numerous studies have developed thermal models of power semiconductor devices, modules, and power electronics systems to extract parameters for predicting temperature ripple [14]–[16]. While these models are useful for estimating the peak-to-peak temperature ripple under various operating conditions, they typically base their predictions on assumed values for chip-level power dissipation. They do not generally connect this power loss to the instantaneous values of current and temperature-dependent electrical resistance that control its value. As a result, their step-change calculations cannot include the effects of changing electrical properties on heat generation. This omission may not be important for kHz-level electrical excitations but can become critical at the low frequencies that motivated this research.

This study revisits the issue of device thermal performance with a specific focus on how temperature-dependent electrical properties influence the transient response of SiC MOSFETS. The first part measures the transient thermal behavior during step changes in the input current. These experiments identify an asymmetrical thermal time constant that depends on whether the step change current applied to the SiC module is increasing or decreasing with time. The second part examines the module thermal response to periodic electrical excitation typical of field applications. These measurements quantify thermal ripple as a function of excitation amplitude and frequency. They also connect the observed dynamic response to the thermal step-change assessment that produced the thermal time constant. Experiments in both parts are complemented by theoretical analyses that both explain the trends observed and identify design variables that influence device transient thermal response. They also provide a useful, and necessary, transient complement to the steady-state assessments typically performed when selecting thermal management solutions in different power electronics applications.

II. Module Description and Experimental Setup

GE Global Research has been active in fundamental SiC research for many years, producing next generation dies that are far superior to their silicon-based counterparts. Recently, GE developed a high current switch which integrates multiple GE-designed SiC die into an *EconoDual* package [17]. The 4.5 by 4.5 mm GE die are vertical SiC MOSFETS with an aluminum source (topside) and gold drain (backside) capable of supporting 1700 V/240 A. The integrated package uses an aluminum nitride direct bonded copper substrate, copper baseplate, laminated copper plus/minus bus bar layered with a Kapton polyimide film, and a Ryton housing. The modules support a range of currents and offer a low cost, low induction solution for numerous power electronics applications.

The thermal experiments performed in this study mounted the module shown in Fig. 1 to a liquid-cooled cold plate through a 100 μm layer of high thermal conductivity thermal interface material (see Fig. 2). They then connected this cold plate to an external fluid chiller, which circulated a temperature-controlled 50–50 mixture of ethylene glycol and water during the experiments. This chiller used internal control logic to regulate coolant temperature to within ±0.5 °C and a ball valve to control the coolant flow rate as tracked to within ±2% using an inline

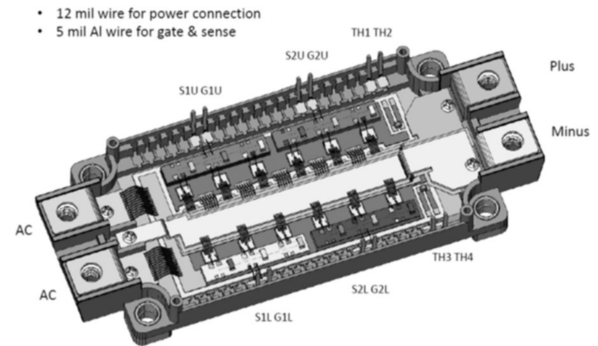

Fig. 1. GE 1700V/240A SiC power module.

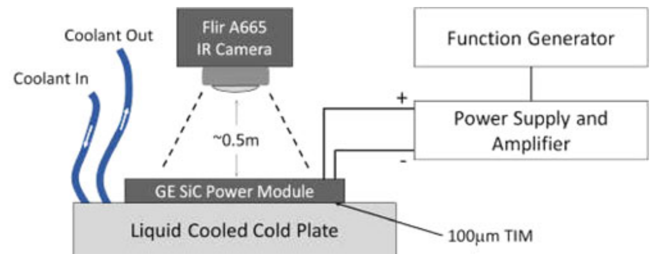

Fig. 2. Experimental setup: GE SiC power module, cold-plate, IR camera, and power.

flowmeter. The setup removed the module cover and dielectric gel and sprayed the exposed die with a matt black paint of known emissivity to enable temperatures to be accurately measured using infrared thermography. The entire assembly was positioned below a FLIR A-665 Infrared Camera (IR) that sampled thermal images at 50 Hz, allowing each test to provide usable temperature data for excitation frequencies up to about 10 Hz.

The experiments energized the dies in the module with I^2R Joule heating provided through an applied controlled current. They connected the upper and lower switch dc buses to a 20 V–750 A power supply with heavy duty cables. The power supply was then connected to a function generator that provided the unsteady current excitation needed for each test. The power supply had a slew rate of 5 ms, allowing it to provide precise changes in excitation current used for each electrical load.

The thermal tests were sequenced so that the stable state at one excitation became the known initial condition value for the next. Each test established the current excitation to be examined and gave the system 5 min to reach a stable thermal state. The IR camera recorded 500 images of module temperatures at 50 Hz to provide 10 s of transient data for each operating scenario (see Fig. 3). By adding a “region-of-interest” box to the IR images, the camera software could extract time histories of temperature at specific regions of the module that could then be interrogated to extract module transient thermal performance. The quoted uncertainty in the absolute temperature provided by the IR camera is ±2 °C.

III. Transient Thermal Response to Step Change Excitation

The first part of this study examined the thermal time constant of the module by subjecting it to step changes in excitation current. The thermal time constant is typically defined as the

Fig. 3. Example IR thermal image of a GE SiC module.

time required for its normalized transient response to reach within e^{-1} of steady state. Its value is usually obtained from temperature data cast in the dimensionless form given by the following equation:

$$\frac{T(t) - T_{\text{Initial}}}{T_{\text{Final}} - T_{\text{Initial}}} = 1 - \exp\left(-\frac{t}{\tau}\right). \quad (1)$$

In this expression, T_{Initial} refers to the initial temperature, T_{Final} is the steady-state final temperature, and $T(t)$ is the temperature at time t. Equation (1) implicitly assumes the thermal system has a classic first-order transient response that is characterized by a single time constant τ obtained from data by setting $t = \tau$

$$\frac{T(\tau) - T_{\text{Initial}}}{T_{\text{Final}} - T_{\text{Initial}}} = 1 - e^{-1} = 0.632. \quad (2)$$

The thermal time constant τ is the product of thermal capacitance C_{Th} and thermal resistance R_{Th}

$$\tau = C_{\text{Th}} R_{\text{Th}} = (\rho c V)\left(\frac{1}{hA}\right) \quad (3)$$

where ρ is the density, c is the specific heat, V is the volume, h is the convective heat transfer coefficient, and A is the surface area. Even if the assumptions behind (1) do not apply in this study, (2) can still define a "time constant" that can be used to assess module thermal performance.

In the thermal time constant tests, the system established a steady coolant flow and energized the module to a base current that would set the initial condition (150 A for a step-up test and 210 A for a step-down test). After allowing temperatures to reach steady state, the test commanded the power supply to produce a step change in current, either up or down as appropriate. It then recorded 10 s of IR video at 50 frames/s to track module temperatures as a function of time. These frames were then interrogated as described above to extract the transient thermal information of interest here. The experiments considered coolant flow rates from 3.2 to 13.3 liter/min (lpm) for an inlet coolant temperature of 40 °C.

Figs. 4 and 5 present measured temperatures for the hottest die on the module as a function of coolant flow rate for step increases and step decreases in current, respectively. The shifts in die temperature curves reflect the differences in convective heat transfer coefficient that accompany changes in the coolant flow rate. They also show how die steady-state temperatures

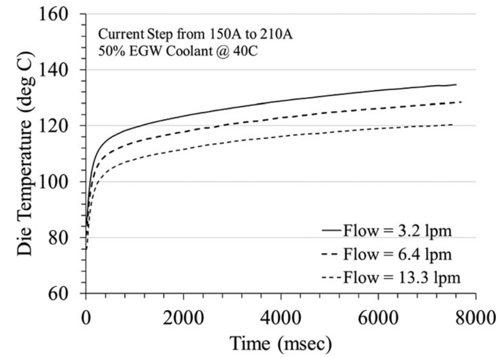

Fig. 4. Die temperatures during step increase in current.

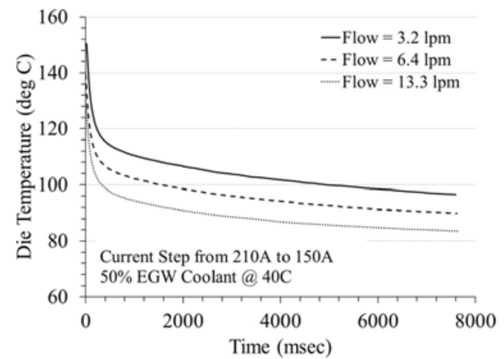

Fig. 5. Die temperatures during step decrease in current.

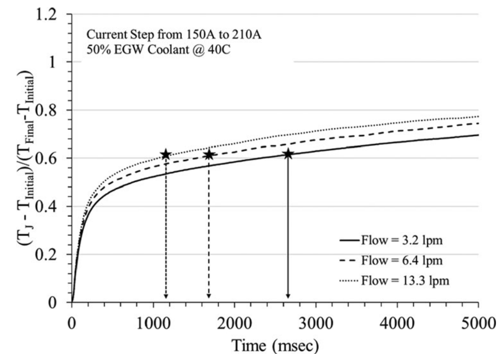

Fig. 6. Dimensionless die temperatures during step increase in current.

vary with flow rate, with a spread of about 20 °C for the values considered here.

Figs. 6 and 7 recast the data presented in Figs. 4 and 5 in the dimensionless form (1) requires to extract the thermal time constant. The stars on each curve identify the thermal time constant as defined by (2) for each test scenario. For both step increases and step decreases in current, the time constant increases as the coolant flow rate decreases. As (3) suggests, the decrease in convective heat transfer coefficient h that accompanies a decrease in coolant flow rate increases the thermal resistance R_{Th} and increases the thermal time constant. This behavior is displayed in Figs. 6 and 7, which both show the thermal time constant doubling as the flow rate goes from 3.2 to 13.3 lpm.

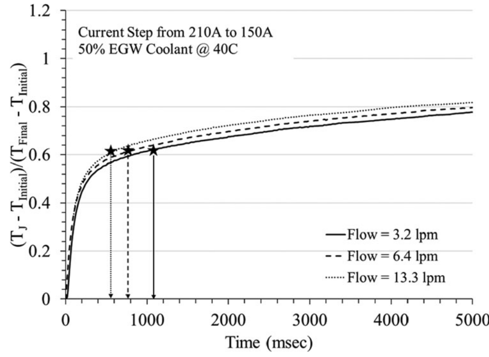

Fig. 7. Dimensionless die temperatures during step decrease in current.

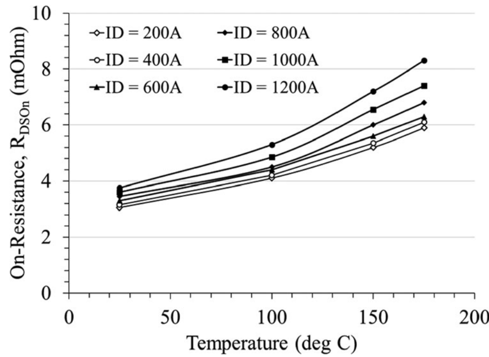

Fig. 8. Variation of module electrical resistance with temperature.

The temperature plots in Figs. 6 and 7 also show that the thermal time constant is sensitive to whether the current is increasing or decreasing. This result was unexpected, as (3) shows the time constant only depends on thermal capacitance and thermal resistance, neither of which varied during the step-change tests. Instead, the plots suggest the time constant of the module during a step increase in current is two-to-three times higher than the value observed during a step decrease in current.

The source of the unexpected link between current change and time constant can be traced to the temperature dependency of the electrical resistance in the module (see Fig. 8). Consider a lumped system in which a volume of material having density ρ, specific heat c, and volume V is heated internally by a heat source Q and cooled externally by convection to an ambient T_A with convective coefficient h. The temperature of this lump is governed by a first-order differential equation derived using an energy balance

$$\rho V c \frac{dT}{dt} = Q - hA\left(T - T_A\right). \quad (4)$$

In the case relevant to this study, the heat generation rate Q is given by the following equation:

$$Q = I^2 R \quad (5)$$

where I is the current and R is the resistance, which is a function of temperature (see Fig. 8)

$$R = R_0 + R_1 T + R_2 T^2. \quad (6)$$

Combining (4) to (6) yields the following:

$$\rho V c \frac{dT}{dt} = \pm I^2 \left(R_0 + R_1 T + R_2 T^2\right) - hA\left(T - T_A\right) \quad (7)$$

where the upper symbol in front of current represents heating (current increase) and the lower symbol in front of current represents cooling (current decrease). For the case with $R_1 = R_2 = 0$, (7) reduces to the familiar differential equation for constant heat source

$$\rho V c \frac{dT}{dt} = \pm Q_0 - hA\left(T - T_A\right) \quad (8)$$

with $Q_0 = I^2 R_0$. The temperature time history in this case is given by (1) with time constant given by (3). This time constant does not vary with temperature or whether the current is increasing or decreasing. If, however, the resistance R in (5) is a linear function of temperature ($R_2 = 0$), (7) becomes as follows:

$$\rho V c \frac{dT}{dt} = \pm I^2 \left(R_0 + R_1 T\right) - hA\left(T - T_A\right) \quad (9)$$

which, with algebra, can be rearranged to the following:

$$\rho V c \frac{dT}{dt} = \pm Q_0^{\dagger} - (hA)^{\dagger}\left(T - T_A\right) \quad (10)$$

where

$$Q_o{}^{\dagger} = \pm I^2 \left(R_0 + R_1 T_A\right) \quad (11)$$

and

$$(hA)^{\dagger} = hA \mp I^2 R_1. \quad (12)$$

Equation (10) is the same as (8) for constant values of heat generation and convective coefficient. As a result, the time constant is still given by (3) but with *hA* now given by (12)

$$\tau_{\text{Heating}} = \frac{\rho c V}{hA - I^2 R_1} \quad (13)$$

and

$$\tau_{\text{Cooling}} = \frac{\rho c V}{hA + I^2 R_1}. \quad (14)$$

These expressions show that the temperature dependency of the resistance R introduces an additional term to the thermal time constant. This term reduces the effective convective coefficient during current increase and increases the effective convective coefficient during current decrease. As a result, the time constant for current increase is longer than that for current decrease, exactly the trend displayed by the data.

The case for which R_2 is not zero is a little more complicated but still displays the thermal time constant hysteresis suggested by the test data. With a little algebra, (7) can be recast in the form again given by (10)

$$\rho V c \frac{dT}{dt} = \pm Q_0^{\dagger\dagger} - (hA)^{\dagger\dagger}\left(T - T_A\right). \quad (15)$$

This time, the equivalent heat source and convection conductance are given by the following equation:

$$Q_o{}^{\dagger\dagger} = \pm I^2 \left(R_0 + R_1 T_A + R_2 T_A^2\right) \quad (16)$$

and

$$(hA)^{\dagger\dagger} = hA \mp I^2 R_1 \mp I^2 R_2\left(T + T_A\right). \quad (17)$$

TABLE I
CURVE FIT COEFFICIENTS FOR THREE-TIME-CONSTANT THERMAL RESPONSE

	Cooling			Heating		
Flow (L/min)	13.3	6.4	3.3	13.3	6.4	3.3
C_1	0.54	0.51	0.52	0.47	0.44	0.41
C_2	0.18	0.15	0.12	0.17	0.12	0.12
C_3	0.29	0.35	0.36	0.36	0.44	0.48
τ_1	0.11	0.094	0.13	0.12	0.12	0.12
τ_2	1.34	1.03	1.44	1.40	1.01	1.06
τ_3	10.8	9.14	10.4	10.3	9.28	11.3

In this case, the solution is no longer given by (1) but one can expect the time constant to include contributions from the R_2 term. In particular, (13), (14), and (17) suggest the time constant will vary with temperature, further complicating evaluation of module transient response.

The analysis to this point has assumed that the transient response of the module is represented by a single time constant τ. When overlaid on Figs. 6 and 7, however, the first-order response given by (1) does not match the data very well. Instead the curves suggest that the observed transient response is determined by contributions whose importance changes with time. To see whether this interpretation is reasonable, the study fit a curve of the form given by (18) to the data in Figs. 6 and 7

$$\frac{T(t) - T_{\mathrm{Initial}}}{T_{\mathrm{Final}} - T_{\mathrm{Initial}}} = C_1\left(1 - \exp\left(-\frac{t}{\tau_1}\right)\right) + C_2\left(1 - \exp\left(-\frac{t}{\tau_2}\right)\right) + \cdots. \quad (18)$$

The form of this curve fit was motivated by the layer-by-layer representation of transient thermal response captured by a classic Cauer network (e.g., [15]). While the measurements showed that the transient thermal behavior of the entire assembly was not captured by a single exponential, it seemed reasonable to expect each layer in the stack-up would be. This approach would also make it easier to ascribe a plausible physical interpretation to whatever insight the curve fits provided.

The initial application of (18) to the test data considered multiple exponential-decay terms representing each layer in the die-module-cold plate stack up. The quality of the resulting curve fit, however, did not improve beyond using three terms in the sum. Table I lists the coefficients C_i and time constants τ_i for the best fits of (18) to the data collected for the assembly studied here. A propagation of error analysis [18] suggests the uncertainty in time constants extracted from the temperature measurements is about 15%. Continuing the interpretation of (18) as a Cauer network, the time constant τ_1 is about the magnitude expected for the die. The time constants τ_2 and τ_3 have values consistent with those expected for the module structure and the cold plate, respectively. One may plausibly argue that the τ_1 really represents the die, solder, and substrate, and that τ_2 primarily represents the module baseplate, but the clear difference in the values of the three time constants is the key insight the curve fit provides.

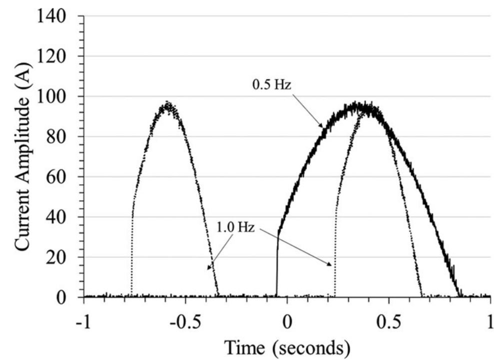

Fig. 9. Example current periodic excitations for transient module thermal test.

IV. TEMPERATURE RIPPLE RESPONSE TO PERIODIC CURRENT EXCITATION

The second part of this study examined the transient thermal response of the SiC module under a periodic current excitation. It was especially interested in quantifying the thermal ripple $\Delta T_{\mathrm{Ripple}}$ that results from transient excitations that occur at the system fundamental frequency. For the purposes of this study, thermal ripple was defined by the following equation:

$$\Delta T_{\mathrm{Ripple}} = T_{\mathrm{Die,Max}} - T_{\mathrm{Die,Min}}. \quad (19)$$

The ripple experiments followed the protocol used for the step-change studies in Section III, but with the step-change excitation replaced with a half-sine wave excitation typical of that expected in future applications. Fig. 9 provides examples of periodic 100 A loads with frequencies of 0.5 and 1.0 Hz. The tests also considered excitation frequencies of 2, 4, and 8 Hz and amplitudes of 150, 200, and 250 A. Beyond 8 Hz, the Nyquist criterion of needing at least four samples per period to preserve excitation frequency would not be satisfied by the 50 Hz sampling rate of the IR camera used for the temperature measurements.[1] For a given amplitude, the total heat dissipated per unit time is independent of frequency. The frequency merely affects how this heat dissipation is introduced to the SiC module over time, and not its time-averaged value. As a result, the time-averaged die temperature observed for each amplitude was the same, even though the time histories at each frequency were quite different.

Fig. 10 presents thermal ripple measured for the module excited with a 250 A periodic signal at frequencies of 0.5, 1, and 4 Hz. The amplitude of the die temperature fluctuation decreases with the increasing excitation frequency. Fig. 11 translates the data in Fig. 10 to an equivalent thermal ripple (19) and adds in data collected for the other frequencies and amplitudes considered in this study. The curves show that ripple magnitude increases with the increasing excitation amplitude but decreases with the increasing frequency. The data also suggest that excitations at frequencies beyond ~10 Hz will not produce significant levels of ripple. This frequency estimate is consistent with the

[1]The response time of the Magna-Power power supply also introduces a step change in current during the transient but this is not expected to affect the periodic excitation applied to the module during the thermal test.

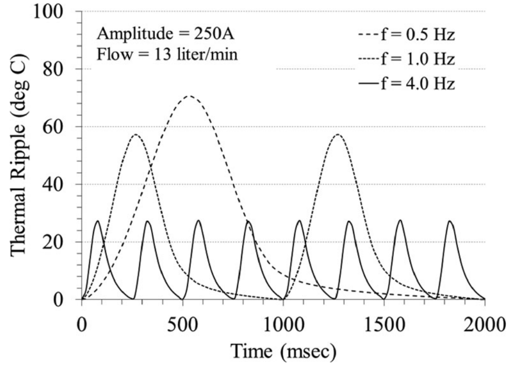

Fig. 10. Transient component of die temperature for 250 A at three frequencies.

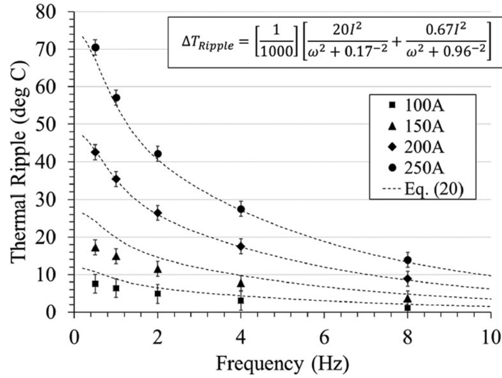

Fig. 11. Temperature ripple as a function of excitation frequency and current.

100 ms thermal time constant observed for the die in the previous section; electrical excitations with periods shorter than the die thermal time constant will produce very little ripple.

Additional insight into the factors that influence thermal ripple can be identified by extending the lumped thermal model presented in Section III to a periodic excitation. If the steady heat source Q in (4) is replaced with a periodic heat source $Q(t) = I^2 R\sin(\omega t)$, it can be shown that the periodic lump temperature time history is given notionally by the following equation:

$$T(t) \sim \frac{I^2}{\omega^2 + \tau^{-2}} \left[\frac{\sin(\omega t)}{\tau} - \omega\cos(\omega t)\right] \tag{20}$$

where τ is the thermal time constant defined by (3). This expression shows that the amplitude of the thermal ripple depends on excitation frequency ω and excitation amplitude I^2 as well as the module thermal design τ. It also suggests that for a given value of τ, the amplitude of thermal ripple decreases with roughly the inverse of excitation frequency ω.

Fig. 11 overlays curves having a superposition form of (20) against the ripple data collected in this study. The curve fit to the amplitude premultiplier in (20) provided in the inset shows the time constants notionally representing the die and module influence ripple, with τ-values on the same order as those listed in Table I. Expanding the fit to include a third time constant has little effect on the fit, and the $\sim$10 s time constant of the cooling system is too long to affect the thermal ripple. Although the excitation used in the experiment is different from the single-term sinusoid assumed in the model, the excellent agreement between (20) and the test data suggests its form is reasonable.

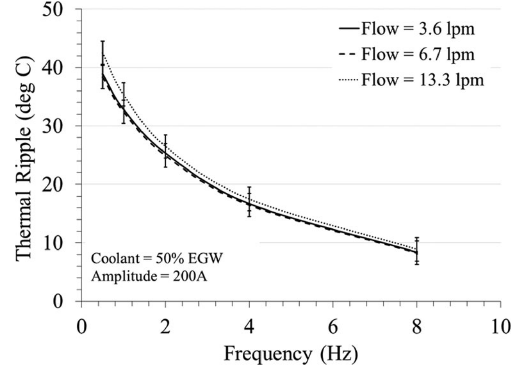

Fig. 12. Influence of coolant flow rate on thermal ripple.

The step-change results presented in Section III showed that the coolant flow rate affected both the thermal time constant of the assembly and the steady-state temperature the module achieved at each thermal load. To see whether this flow rate influence also carried over to periodic electrical excitations, the study ran a final experiment to see whether the coolant flow rate also affected thermal ripple. Fig. 12 presents the thermal ripple data for a 200 A periodic excitation as a function of frequency for the coolant flow rates considered in Section III. These results show that the coolant flow rate has almost no effect on the measured ripple, even at the large amplitude considered here. Any change in the coolant flow rate would affect the time constant of the cold plate. As the step change audit in Table I shows, however, the time constant of the cold plate is about 10 s, an order of magnitude longer than the time scales associated with changes in die temperature.

A change in the coolant flow rate would influence a thermal time constant that is too long to influence temperature changes at the die level. More importantly, these results show that it is not possible to reduce thermal ripple by modifying the design of the cold plate; thermal ripple is determined by processes that take place over time scales that are much shorter.

V. Conclusion

This study examined the transient thermal response characteristics of a next-generation SiC power electronics module. The results indicated that thermal transients in these modules are determined by three time constants, one for the die, one for the module, and one for the cold plate to which it is attached. They also suggested the presence of a thermal hysteresis characterized by different time constants during increases and decreases in excitation current. Additional tests in which the modules were excited by periodic current flows showed that the thermal ripple decreased with the increasing excitation frequency and that the periodic response was not affected by the cooling system design.

Taken together, the results obtained here illustrate the importance understanding time-scales when designing electrical–thermal systems and components. Control algorithms, for example, may have to consider thermal hysteresis for assemblies

in which the time scales of electrical excitation and thermal response are comparable. As dies get smaller and thermal packaging improves, the time constants of assemblies will drop to where the frequency at which thermal ripple becomes important will go up. Cold-plate thermal performance does not appear to influence thermal ripple, but an improved design can reduce mean assembly temperatures and provide more margin for temperature peaks during transients. Engineering of next-generation power electronics would benefit from an integrated codesign process that recognizes how electrical and thermal interact to determine system performance.

ACKNOWLEDGMENT

The authors would like to acknowledge the technical support provided by R. Datta, P. Sandvik, and M. Harfman-Todorovic of GE Global Research Niskayuna and A. Chan and T. Schuetz of GE Global Research Munich throughout this project.

REFERENCES

[1] H. Wang, M. Liserre, and F. Blaabjerg, "Toward reliable power electronics: Challenges, design tools, and opportunities," *IEEE Ind. Electron. Mag.*, vol. 7, no. 2, pp. 17–26, Jun. 2013.

[2] K. Ma, M. Liserre, F. Blaabjerg, and T. Kerekes, "Thermal loading and lifetime estimation for power devices considering mission profiles in wind power converter," *IEEE Trans. Power Electron.*, vol. 30, no. 2, pp. 590–602, Mar. 2014.

[3] X. She, A. Q. Huang, O. Lucia, and B. Ozpineci, "Review of silicon carbide power devices and their applications," *IEEE Trans. Ind. Electron.*, 2017.

[4] J. Millan, P. Godignon, X. Perpina, A. P. Tomas, and J. Rebollo, "A survey of wide bandgap power semiconductor devices," *IEEE Trans. Power Electron.*, vol. 29, no. 5, pp. 2155–2163, May 2014.

[5] H. Mantooth, M. G. Glover, and P. Shepherd, "Wind bandgap technologies and their implications on miniaturizing power electronics system," *IEEE J. Emerg. Sel. Topics Power Electron.*, vol. 2, no. 3, pp. 374–385, Sep. 2014.

[6] E. Laloya, O. Lucia, H. Sarnago, and J. M. Burdio, "Heat management in power converters: From state of the art to future ultrahigh efficiency systems," *IEEE Trans. Power Electron.*, vol. 31, no. 11, pp. 7896–7908, Nov. 2016.

[7] W. Han and S. Jeong, "Evaluation of the thermal performance with different fin shapes of the air-cooled heat sink for power electronic applications," *J. Int. Council Elect. Eng.*, vol. 6, no. 1, pp. 17–25, 2016.

[8] G. Kyle., S. Cai., C. Neft, and A. Bhunia, "Liquid jet impingement cooling of a silicon carbide power conversion module for vehicle applications," *IEEE Trans. Power Electron.*, vol. 30, no. 6, pp. 2975–2984, Jun. 2015.

[9] Y. Wang, X. Dai, G. Liu, Y. Wu, D. Li, and S. Jones, "Integrated liquid cooling automotive IGBT module for high temperatures coolant application," in *Proc. Int. Exhib. Conf. Power Electron. Power Electron. Intell. Motion Renewable Energy Manage.*, Nuremberg, Germany, 2015, pp. 1197–1204.

[10] H. Bostanci, D. Ee, B. Saarloos, D. Pini, and L. Chow, "Thermal management of power inverter modules at high fluxes via two-phase spray cooling," *IEEE Trans. Compon., Packag. Manuf. Technol.*, vol. 2, no. 9, pp. 1480–1485, Sep. 2012.

[11] Q. Huang, X. Zou, D. Zhu, and Y. Kang, "Scaled current tracking control for doubly fed induction generator to ride-through serious grid faults," *IEEE Trans. Power Electron.*, vol. 31, no. 3, pp. 2150–2165, Mar. 2016.

[12] D. Zhu, X. Zou, L. Deng, Q. Huang, S. Zhou, and Y. Kang, "Inductance-emulating control for DFIG-based wind turbine to ride through grid faults," *IEEE Trans. Power Electron.*, vol. 32, no. 11, pp. 8514–8525, Nov. 2017.

[13] K. Ma and F. Blaabjerg, "Modulation methods for neutral-point clamped wind power converter achieving loss and thermal redistribution under low-voltage-ride-through," *IEEE Trans. Ind. Electron.*, vol. 61, no. 2, pp. 835–845, Feb. 2014.

[14] A. S. Bahman, K. Ma, and F. Blaabjerg, "Thermal impedance model of high power IGBT modules considering heat coupling effects," in *Proc. Int. Power Electron. Appl. Conf. Expo.*, 2014, pp. 1382–1387.

[15] T. Kojima, Y. Yamada, Y. Nishibe, and K. Torii, "Novel RC compact thermal model of HV inverter module for electro-thermal coupling simulation," in *Proc. Power Convers. Conf.*, 2007, pp. 1025–1029.

[16] P. Evans, A. Castellazzi, and C. Johnson, "Automated fast extraction of compact thermal models for power modules," *IEEE Trans. Power Electron.*, vol. 28, no. 10, pp. 4791–4802, Oct. 2013.

[17] L. Stevanovic *et al.*, "High performance SiC MOSFET module for industrial applications," in *Proc. 28th Int. Symp. Power Semicond. Devices ICs*, 2016, pp. 479–482.

[18] S. J. Kline and F. A. McClintock, "Describing uncertainties in single-sample experiments," *Mech. Eng.*, vol. 75, pp. 3–8, Jan. 1953.

Gary Mandrusiak received the Ph.D. degree in mechanical engineering from the University of California, Berkeley, CA, USA, in 1988.

He is a Senior Research Engineer with the Electronics Cooling Laboratory, General Electric Global Research, Niskayuna, NY, USA. His research interests include microchannel and microjet cooling, power electronics thermal management, next-generation heat sink design, and computational fluid dynamics.

Xu She (S'08–M'13–SM'15) received the B.Sc. degree in electrical engineering and the B.A. degree in english in 2007, the M.Sc. degree in electrical engineering from Huazhong University of Science and Technology, Wuhan, China, in 2009, and the Ph.D. degree in electrical engineering from North Carolina State University, Raleigh, NC, USA, in 2013.

He is a lead electrical Engineer at GE Global Research Center, Niskayuna, NY, USA. His works mainly focus on emerging power electronics technologies, renewable energy systems, and microgrids.

Dr. She was the recipient of the Chinese government award of outstanding graduate student aboard in 2013, the IEEE ECCE Best Paper Award in 2016, and the IEEE Industry Application Society Andrew W. Smith Outstanding Young Member Achievement Award in 2017. His Ph.D. work on solid state transformer was named and cited by MIT technology review as top ten emerging technologies in 2011.

Alistair Martin Waddell received the Ph.D. degree in experimental thermal sciences from the University of Limerick, Limerick, Ireland, in 2015. His doctoral work was part of a collaboration with Bell Labs in a program developing microfluidic cooling for the Photonics devices used in telecommunications networks.

He currently works for GE Global Research, Munich, Germany, and develops cooling systems for MW scale renewables and energy storage products. His research interests include machine electrification and renewable energy technologies.

Sayan Acharya (S'14) received the B.E. degree in electrical engineering from Jadavpur University, Kolkata, India, in 2008, and the M.Tech. degree in electrical engineering from the Indian Institute of Technology, Kharagpur, Kharagpur, India, in 2010. He is currently working toward the Ph.D. degree in electrical engineering at NC State University, Raleigh, NC, USA.

From 2010 to 2013, he was with Emerson Network Power Pvt. Ltd, Thane, India. He joined the FREEDM Systems Center, NC State University in Spring, in 2014. During his Ph.D. study, he worked for GE Global Research Center, Niskayuna, NY, USA, as a research intern. His research interests include wide bandgap device-based power electronics converters, active gate driving techniques for SiC devices, multilevel converters topologies, HVDC, high power converters, multiterminal dc systems, etc.